



Proceeding Paper

# An Iterative Bayesian Algorithm for 3D Image Reconstruction Using Multi-View Compton Data <sup>†</sup>

Nhan Le <sup>1,\*</sup> , Hichem Snoussi <sup>1</sup> and Alain Iltis <sup>2</sup>

<sup>1</sup> LIST3N, Troyes University of Technology, 12 Rue Marie Curie, 10004 Troyes, France; hichem.snoussi@utt.fr

<sup>2</sup> Damavan Imaging, 2 Rue Gustave Eiffel, 10430 Rosières-Près-Troyes, France; alain.iltis@damavan-imaging.com

\* Correspondence: thi-ai-nhan.le@utt.fr; Tel.: +33-3-25-71-84-42

<sup>†</sup> Presented at the 42nd International Workshop on Bayesian Inference and Maximum Entropy Methods in Science and Engineering, Garching, Germany, 3–7 July 2023.

**Abstract:** Conventional maximum likelihood-based algorithms for 3D Compton image reconstruction are often stuck with slow convergence and large data volume, which could be unsuitable for some practical applications, such as nuclear engineering. Taking advantage of the Bayesian framework, we propose a fast-converging iterative maximum a posteriori reconstruction algorithm under the assumption of the Poisson data model and Markov random field-based convex prior in this paper. The main originality resides in developing a new iterative maximization scheme with simultaneous updates following the line search strategy to bypass the spatial dependencies among neighboring voxels. Numerical experiments on real datasets conducted with hand-held Temporal Compton cameras developed by Damavan Imaging company and punctual 0.2 MBq <sup>22</sup>Na sources with zero-mean Gaussian Markov random field confirm the outperformance of the proposed maximum a posteriori algorithm over various existing expectation–maximization type solutions.

**Keywords:** 3D image reconstruction; line search maximization; maximum a posteriori; Markov random field; real Compton data; simultaneous update



**Citation:** Le, N.; Snoussi, H.; Iltis, A. An Iterative Bayesian Algorithm for 3D Image Reconstruction Using Multi-View Compton Data. *Phys. Sci. Forum* **2023**, *9*, 2. <https://doi.org/10.3390/psf2023009002>

Academic Editors: Udo von Toussaint and Roland Preuss

Published: 24 November 2023



**Copyright:** © 2023 by the authors. Licensee MDPI, Basel, Switzerland. This article is an open access article distributed under the terms and conditions of the Creative Commons Attribution (CC BY) license (<https://creativecommons.org/licenses/by/4.0/>).

## 1. Introduction

Compton reconstruction is a method to locate gamma ray sources by measuring a Compton scatter and a photoelectric absorption for each radioactive decay, in terms of positions and deposited energies. The literature of 3D Compton reconstruction methods has been extensively developed following two main streams: (i) *analytical inversion* [1], and (ii) *iterative model-based* [2]. The first stream relies mostly on the relationship between a function and its line integrals. Although it typically leads to fast reconstruction algorithms such as filtered back-projection [3], the accuracy of the resulting reconstructed image is usually limited because of approximations needed in the line-integral model and the inability to take account of uncertainties inherent in photon-limited detection. On the contrary, iterative reconstruction algorithms in the second stream exhibit significant accuracy thanks to the explicit modeling of statistical variations in the photon detection process and the progressive refining of reconstructed images through repetitive calculations. However, the price of this added refinement is the substantially higher computation cost.

In the current state of the art, great interest has put in 3D Compton reconstruction using statistical iterative algorithms [4]. The maximum-likelihood expectation–maximization (MLEM) algorithm and its variants have been the leading statistical iterative reconstruction algorithms for several years. Being applicable for Poisson Compton data in both the bin-mode [5] and list-mode [6], the conventional MLEM algorithm exhibits attractive properties, including consistent and predictable convergence behavior, guaranteed non-negativity, and count preservation at each iteration. Nevertheless, it converges slowly, and requires a large number of Compton events for noise reduction. These two issues are, however, of great

concern for various practical applications, especially in nuclear engineering [7]. A potential solution to these issues is to formulate the 3D reconstruction in the Bayesian framework with a Markov random field (MRF)-based prior, reflecting the smoothness in the expected image. Accordingly, the reconstructed image can be seen as a maximum a posteriori (MaP) estimate from Compton data [2]. Equivalent to the Gibbs distribution [8], the MRF framework provides a simple, yet consistent and highly flexible, formalism for describing the image local structure, where neighboring voxels tend to share similar values [9]. The main difficulty for the MaP estimation with MRF priors is the inseparable neighboring voxels in a so-called energy function that makes a direct application of the conventional EM algorithm generally impossible. To remedy this, the one-step-late method [10] could be used at the risk that the EM algorithm converges to the MAP solution for only certain MRF priors [11]. Another alternative is to replace the energy function by a surrogate enabling separable neighboring voxels [12]. If properly chosen, it can lead to a closed-form update of the EM algorithm even for non-quadratic energies [13]. Additionally, we can also adopt a greedy pixel-wise maximization scheme such as iterative coordinate ascent (ICA) [14] to break interactions among neighboring voxels. Nevertheless, such a sequential greedy maximization is often time consuming due to the large number of voxels considered in 3D reconstruction.

Motivated by the Bayesian framework advantages, our aim is to develop a fast-converging iterative MaP reconstruction algorithm called LMMRFMaP under the assumption of the list-mode Poisson data model and MRF-based convex prior. This LMMRFMaP algorithm separates interactive voxels in a similar way as the ICA [14]; however, in the maximization process, a new simultaneous update with line search is proposed for all voxels, rather than sequentially updating voxels one by one. This improvement allows us to very quickly locate radioactive sources from the list-mode Compton data space, especially when compared with the extended LMMLEM (eLMMLEM) algorithm [15] and the so-called LMMaPEM algorithm developed in [12].

The remainder of the paper is organized as follows. On the basis of the Poisson data model, in Section 2, we develop the LMMRFMaP algorithm for MRF-based convex priors. Numerical experiments and comparative studies conducted with hand-held Temporal Compton cameras developed by Damavan Imaging company and punctual 0.2 MBq  $^{22}\text{Na}$  sources are next introduced and analyzed in Section 3. Finally, the paper ends with some conclusions and perspectives in Section 4.

## 2. LMMRFMaP Algorithm

This section is dedicated to formulating a new MaP algorithm for 3D reconstruction from a list-mode Compton data-space  $L$ . For convenience, we first conduct the formulation under the bin-mode data, as in [16], then derive the model of interest by considering list-mode data as a limiting case of bin-mode data when the bin-widths tend to zero. Thus, we define, for the bin-mode data, a vector of measurements  $\mathbf{g}$ , where each element  $g_i$ ,  $i \in \mathcal{I}$ , describes the random number of counts in a virtual bin  $i$  corresponding to the event  $A_i$  of  $L$ . When  $g_i \rightarrow 1$ ,  $\forall i \in \mathcal{I}$ , then the bin-mode data return to the list-mode ones [17].

We denote  $\mathbf{f}$  the source distribution in the considered image volume  $V$ , where each element  $f_j$ ,  $\forall j \in \mathcal{J}$ , characterizes the emission intensity of the voxel  $v_j$  in  $V$ . Under the Bayesian framework, the 3D reconstruction reduces to find the MaP estimate  $\hat{\mathbf{f}}_{\text{map}}$  of  $\mathbf{f}$ , such that

$$\hat{\mathbf{f}}_{\text{map}} = \arg \max_{\mathbf{f} \geq 0} \{ \mathcal{L}(\mathbf{g} | \mathbf{f}) + \mathcal{L}(\mathbf{f}) \}, \quad (1)$$

where  $\mathcal{L}(\mathbf{f})$  and  $\mathcal{L}(\mathbf{g} | \mathbf{f})$  are the log-prior and log-likelihood functions.

Through a MRF model, we introduce the image smoothness as prior knowledge in estimating  $\mathbf{f}$ . We thus define a *neighborhood system*  $\delta_j$  of the voxel  $v_j$ ,  $\forall j \in \mathcal{J}$ , such that

- $v_j$  cannot be a neighbor of itself (i.e.,  $v_j \notin \delta_j$ );
- If  $v_j$  is a neighbor of  $v_l$ , then  $v_l$  must be a neighbor of  $v_j$  (i.e.,  $v_j \in \delta_l \Leftrightarrow v_l \in \delta_j$ ).

Each system  $\delta_j$  corresponds to a set of *pair-wise* cliques  $\mathcal{C}_j \triangleq \{(v_j, v_l) : v_j \in \delta_l\}$  consisting of all *unordered* neighboring voxels pairs  $(v_j, v_l)$  satisfying  $v_j \in \delta_l$ . Using these notions, we can formulate the log-prior function as [18]

$$\mathcal{L}(\mathbf{f}) = - \sum_{j=1}^J \sum_{(v_j, v_l) \in \mathcal{C}_j} \beta_{jl} \cdot \rho(f_j - f_l), \tag{2}$$

where  $\beta_{jl}$  denotes the model parameter, and  $\rho(\cdot)$  is a *convex* potential function (see [19] for a detailed discussion about different choices of  $\rho(\cdot)$ , and their meanings and properties). Assuming now the Poisson event-counting model for  $g_i$ , we arrive at the log-likelihood function [2]

$$\mathcal{L}(\mathbf{g} | \mathbf{f}) = \sum_{i=1}^I \left( - \sum_{j=1}^J t_{ij} f_j + g_i \ln \left( \sum_{j=1}^J t_{ij} f_j \right) - \ln(g_i!) \right), \tag{3}$$

where  $t_{ij}$  denotes an element of the *system* response matrix indexed on the event  $A_i$  and on the voxel  $v_j$  [15]. Obviously, inseparable  $f_j, \forall j \in \mathcal{J}$  in  $\mathcal{L}(\mathbf{f})$  and  $\mathcal{L}(\mathbf{g} | \mathbf{f})$  make a direct resolution of (1) mathematically intractable. A well-known technique to overcome this obstacle is to replace  $\mathcal{L}(\mathbf{f})$  and  $\mathcal{L}(\mathbf{g} | \mathbf{f})$  by surrogate functions [12,13]. While an efficient log-likelihood surrogate can be easily found thanks to the common assumption of the Poisson data model, a relevant choice for log-prior surrogate is not always straightforward and closely dependent on the specific adopted prior [20]. That is why we propose substituting only  $\mathcal{L}(\mathbf{g} | \mathbf{f})$  by an appropriate surrogate, keeping  $\mathcal{L}(\mathbf{f})$  as it is, and then developing an iterative scheme to maximize the new objective function.

In [20], Bouman proved that the  $Q$ -function in the E-step of the EM algorithm could be an appropriate log-likelihood surrogate for the Poisson data. Sharing their viewpoint, we adapt the  $Q$ -function in our eLMMLEM algorithm [15], and obtain a surrogate of  $\mathcal{L}(\mathbf{g} | \mathbf{f})$  in list-mode (i.e.,  $g_i \rightarrow 1, \forall i \in \mathcal{I}$ ) as

$$Q_l(\mathbf{f}; \mathbf{f}') = \sum_{i=1}^I \sum_{j=1}^J \left( \frac{t_{ij} f'_j}{\sum_{s=1}^J t_{is} f'_s} \ln(t_{ij} f_j) - t_{ij} f_j \right), \tag{4}$$

where  $\mathbf{f}'$  denotes any possible information from earlier iterations, and  $f'_j, \forall j \in \mathcal{J}$ , are elements of  $\mathbf{f}'$ . Using (2) and (4), equivalences of (1) for the list-mode data are obtained by

$$\hat{\mathbf{f}}_{\text{map}} = \arg \max_{\mathbf{f} \geq 0} \{ \mathcal{L}_{\text{map}}(\mathbf{f}) \}, \tag{5}$$

$$\mathcal{L}_{\text{map}}(\mathbf{f}) = \sum_{i=1}^I \sum_{j=1}^J \left( \frac{t_{ij} f'_j}{\sum_{s=1}^J t_{is} f'_s} \ln(t_{ij} f_j) - t_{ij} f_j \right) - \sum_{j=1}^J \sum_{(v_j, v_l) \in \mathcal{C}_j} \beta_{jl} \cdot \rho(f_j - f_l). \tag{6}$$

It is easy to verify that  $\mathcal{L}_{\text{map}}(\mathbf{f})$  is a concave function when the potential function is convex. This leads to the line search maximization scheme with simultaneous update as follows.

**Theorem 1.** *If  $\mathcal{L}_{\text{map}}(\mathbf{f})$  is concave, then the following iterative schema converges to its maximum*

$$\hat{\mathbf{f}}^{(k+1)} \leftarrow \hat{\mathbf{f}}^{(k)} + \sum_{j=1}^J a_j^{(k)} \mathbf{e}_j^{(k)}, \tag{7}$$

where  $\mathbf{e}_j^{(k)} \in \mathbb{R}^J$  is vector whose  $j$ -th component is 1, remainders are 0, and  $a_j^{(k)}$  is given by

$$a_j^{(k)} \leftarrow \arg \max_{a_j \in \mathbb{R}} \{ \mathcal{L}_{\text{map}}(\hat{\mathbf{f}}^{(k)} + a_j \mathbf{e}_j^{(k)}) \}, \quad \forall j \in \mathcal{J}. \tag{8}$$

**Proof.** This theorem is easily proved by applying the Taylor expansion to the  $\mathcal{L}_{\text{map}}(\mathbf{f})$  concave function.  $\square$

The above iterative maximization scheme requires a starting point  $\hat{\mathbf{f}}^{(0)}$ . As in [21], a potential choice for  $\hat{\mathbf{f}}^{(0)}$  is such that  $\hat{f}_j^{(0)} = \sum_{i=1}^I t_{ij}, \forall j \in \mathcal{J}$ .

### 3. Numerical Experiments and Comparative Studies

To assess the performance of the proposed LMMRFMaP algorithm, we set up an experimental system with a punctual 0.2 MBq  $^{22}\text{Na}$  source and a hand-held Temporal Compton camera developed by the Damavan Imaging company.

The camera is sequentially deployed at three different view-angles, as in Figure 1: *the two first views are set perpendicularly on a same horizontal plane  $\mathbf{H}$  of the punctual source, and the third view is placed vertically above.* The distance between the camera and the source is 500 mm, and the whole system is located 500 mm from the ground. We conducted the acquisition within 15 min to constitute different list-mode data-spaces  $L$  for comparative studies among the eLMMLEM, LMMaPEM, and LMMRFMaP algorithms.

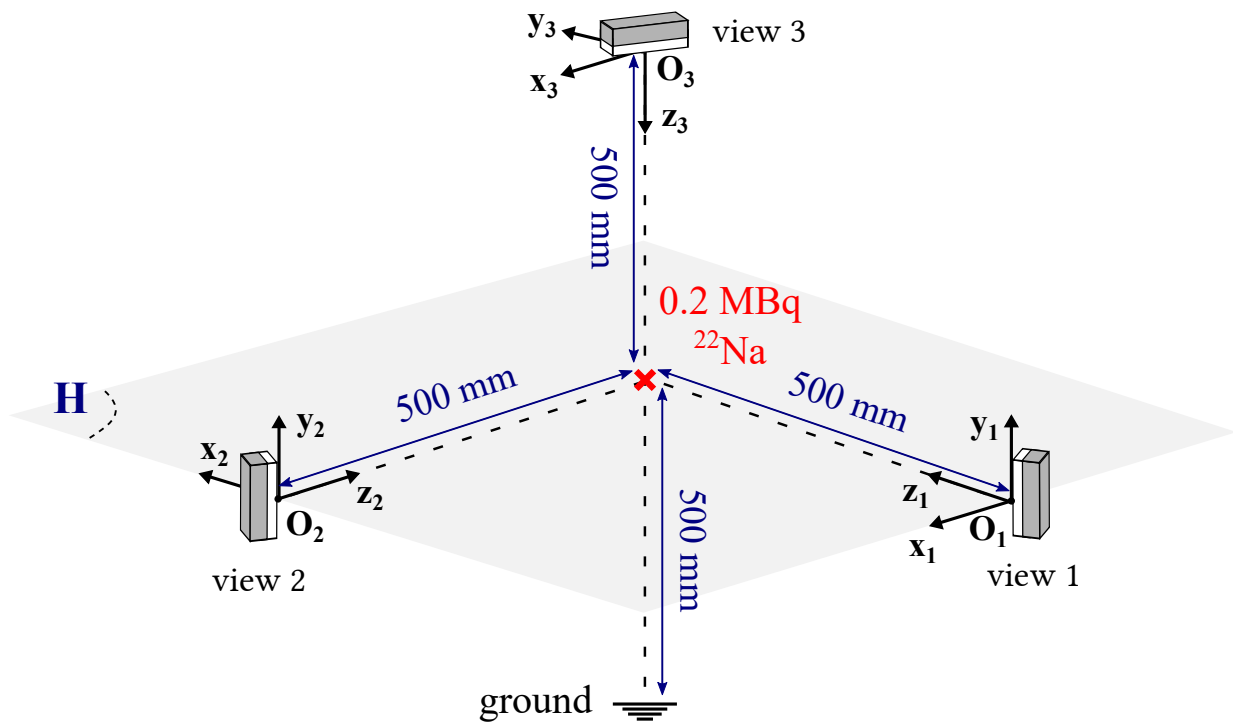


**Figure 1.** Experiment setting for Compton data acquisition.

Assuming the uniform sensitivity for the camera system, the eLMMLEM algorithm always admits the closed-form update at the  $(k + 1)$ -st iteration as

$$\hat{f}_{\text{mle},j}^{(k+1)} \leftarrow \hat{f}_{\text{mle},j}^{(k)} \sum_{i=1}^I \frac{t_{ij}}{\sum_{s=1}^J t_{is} \hat{f}_{\text{mle},s}^{(k)}}, \quad \forall j \in \mathcal{J}, k \in \mathbb{N}. \tag{9}$$

Unlike the eLMMLEM algorithm, the update form of the LMMaPEM and LMMRFMaP algorithms depends closely on the choice of prior model. To enable their closed-form update, we choose the zero-mean Gaussian MRF with the potential function  $\rho(f_j - f_l) = \frac{1}{2}(f_j - f_l)^2$  for describing the local smoothness of the expected reconstructed image. This choice gives the updates at the  $(k + 1)$ -st iteration as

- For the LMMaPEM algorithm:

$$\hat{f}_{\text{mapem},j}^{(k+1)} \leftarrow \frac{1}{8} \sqrt{\left(1 - 2 \left( \hat{f}_{\text{mapem},j}^{(k)} + \sum_{(v_j, v_l) \in \mathcal{C}_j} \beta_{jl} \hat{f}_{\text{mapem},l}^{(k)} \right)\right)^2 + 16 \sum_{i=1}^I \frac{t_{ij} \hat{f}_{\text{mapem},j}^{(k)}}{\sum_{s=1}^J t_{is} \hat{f}_{\text{mapem},s}^{(k)}} - \frac{1}{8} \left(1 - 2 \left( \hat{f}_{\text{mapem},j}^{(k)} + \sum_{(v_j, v_l) \in \mathcal{C}_j} \beta_{jl} \hat{f}_{\text{mapem},l}^{(k)} \right)\right)}, \quad \forall j \in \mathcal{J}, k \in \mathbb{N}, \quad (10)$$

- For the LMMRFMaP algorithm:

$$\hat{f}_{\text{mrfmap},j}^{(k+1)} \leftarrow \frac{1}{2} \sqrt{\left(1 - \sum_{(v_j, v_l) \in \mathcal{C}_j} \beta_{jl} \hat{f}_{\text{mrfmap},l}^{(k)}\right)^2 + 4 \sum_{i=1}^I \frac{t_{ij} \hat{f}_{\text{mrfmap},j}^{(k)}}{\sum_{s=1}^J t_{is} \hat{f}_{\text{mrfmap},s}^{(k)}} - \frac{1}{2} \left(1 - \sum_{(v_j, v_l) \in \mathcal{C}_j} \beta_{jl} \hat{f}_{\text{mrfmap},l}^{(k)}\right)}, \quad \forall j \in \mathcal{J}, k \in \mathbb{N}, \quad (11)$$

where  $\sum_{(v_j, v_l) \in \mathcal{C}_j} \beta_{jl} = 1$ , and the pair-wise clique  $\mathcal{C}_j$  is chosen as in [22] (i.e.,  $\mathcal{C}_j$  consists of the eight nearest voxels from the same slice and the single nearest voxels of the upper and lower slices). The updates (9)–(11) also require a probabilistic model for  $t_{ij}$ . In this work, we adapt Maxim et al.’s model [23] for Compton data by adding different measurement uncertainties related to the spatial and energy resolution of detectors, as well as the Doppler broadening effect to make the model more flexible.

To see how fast the LMMRFMaP algorithm is when compared to the eLMMLEM and LMMaPEM algorithms, we fix the number of events at  $I = 20$  events/view and observe the evolution of the associated reconstructed 3D images at the  $k$ -th iteration with  $k = 1, 3, 5, 7$ . Visually, we can find from Figure 2 that the point cloud returned by the LMMRFMaP algorithm converges to true punctual source (marked by the red cross) much faster than the one returned by the two other algorithms.

Quantitatively, we propose using the so-called *sum of weighted distances* (SWD) between the reconstructed point cloud and the true source as a measure for the quality assessment at the  $k$ -th iteration

$$\text{SWD}^{(k)} = \sum_{j=1}^J \hat{f}_j^{(k)} \|P_j - P_S\|_2, \quad (12)$$

where  $\hat{f}_j^{(k)}$  is given either from (9), (10) or (11);  $P_j$  and  $P_S$  are, respectively, the coordinate vectors of the voxel  $v_j$  and the punctual source; and  $\|\cdot\|_2$  standards for the Euclidean norm. The SWD exhibits a compromise between the intensity of the voxels and their accuracy with respect to the source location. The lower the value of  $\text{SWD}^{(k)}$ , the nearer the reconstructed 3D image is to the true source. Fixing the number of events at  $I = 20$  events/view, we randomly build 100 list-mode data-spaces, reconstruct the images of punctual source following (9)–(11), and compute the associated SWD following (12). Next, we sketch the evolution of the mean and the standard deviation of these SWD with respect to the iteration number  $k$  in Figure 3a. Clearly, the proposed LMMRFMaP algorithm exhibits a higher convergence speed and higher reconstruction quality than the LMMaPEM and eLMMLEM algorithms. Similarly, we fix the iteration number at  $k = 5$ , and vary the number of events/view from 4 to 20 with step 4 to evaluate the impact of the events number on the reconstruction performance. Indeed, for each of these configurations, we also build 100 list-mode data-spaces, compute the associated SWD for the considered algorithms, then sketch in Figure 3b the evolution of their mean and standard deviation.

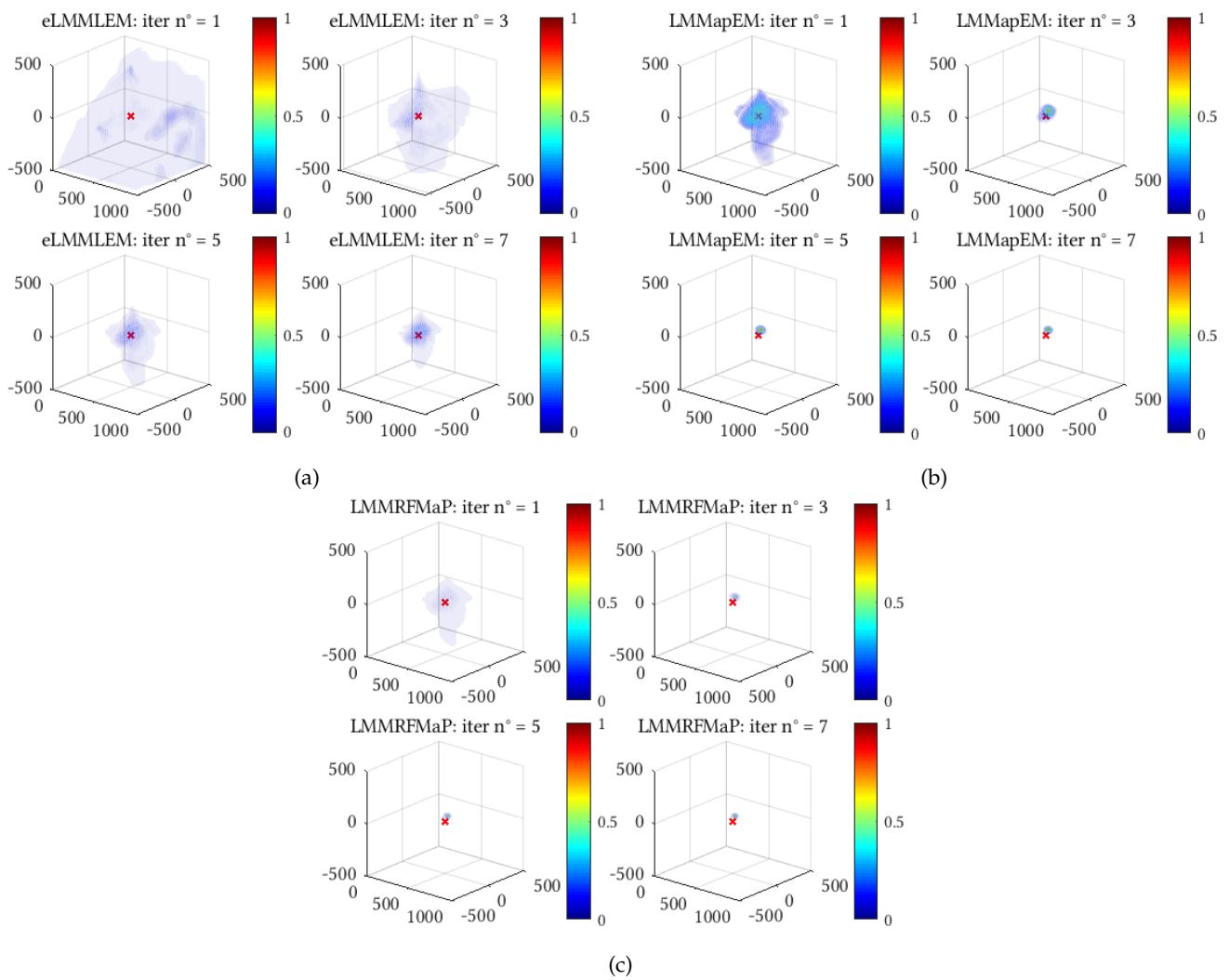


**Figure 2.** Evolution of point clouds returned by the considered algorithms (20 events/view): (a) eLMMLEM algorithm, (b) LMMaPEM algorithm, (c) LMMRFMaP algorithm.

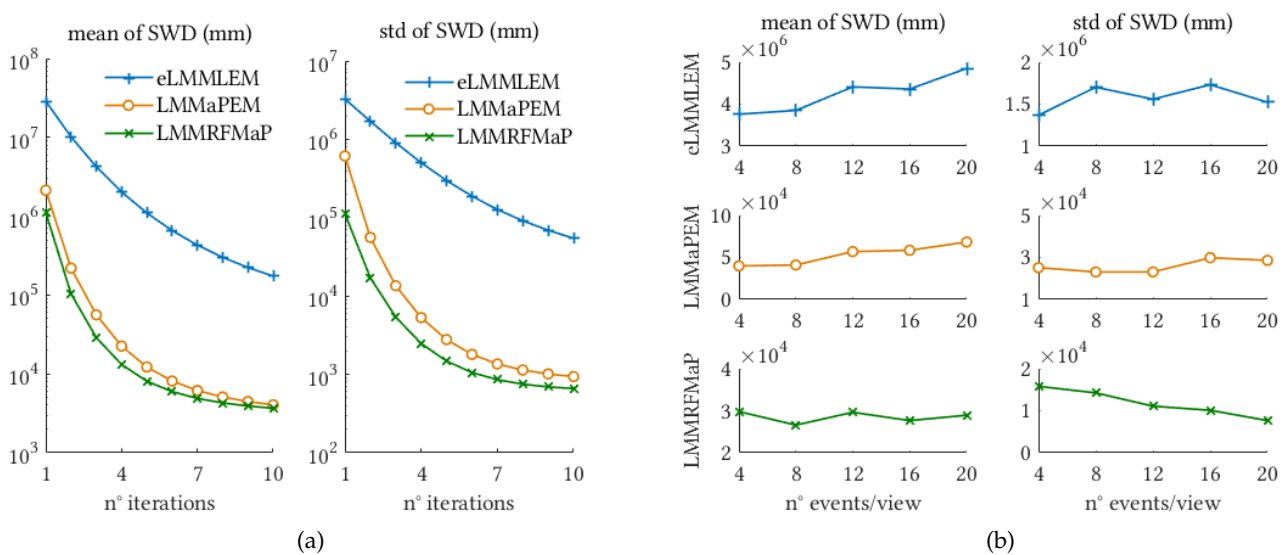


**Figure 3.** Evolution of the mean and the standard deviation of SWD: (a) evolution with respect to the number of iterations, (b) evolution with respect to the number of events/view.

We can remark that the mean values of SWD given by the LMMRFMaP algorithm are more-or-less constant when the number of events/view varies, while the ones given by the LMMaPEM and eLMMLEM algorithms present a growing trend. This means that the LMMRFMaP algorithm does not require as large a number of events/view to obtain as good a convergence as the two other algorithms. Of course, as shown by the curve of SWD standard deviation, the higher the number of events/view, the more precise the reconstruction results are.

#### 4. Conclusions and Perspectives

Using the Bayesian framework, in this paper, we proposed the LMMRFMaP algorithm for 3D reconstruction from list-model Compton data. Various comparative studies with more classical statistical reconstruction algorithms on three-view real Compton data confirm that the algorithm can very quickly return an accurate image of a punctual radioactive source with a small number of events/view. These advantages are gained thanks to a novel line search maximization scheme with simultaneous updates developed for MRF-based convex priors. Based on these promising results, ongoing work is devoted to more exhaustive testing of the algorithm performances with other kinds of radioactive sources, such as multiple point sources and extended sources. Another perspective is to extend the proposed algorithm for other kinds of MRF-based priors (e.g., non-convex, mixtures, etc.).

**Author Contributions:** Conceptualization, N.L., H.S. and A.I.; methodology, N.L. and H.S.; software, N.L.; validation, N.L., H.S. and A.I.; formal analysis, N.L.; investigation, N.L., H.S. and A.I.; resources, N.L., H.S. and A.I.; data curation, N.L. and A.I.; writing—original draft preparation, N.L.; writing—review and editing, N.L., H.S. and A.I.; visualization, N.L.; supervision, H.S.; project administration, H.S. and A.I.; funding acquisition, H.S. and A.I. All authors have read and agreed to the published version of the manuscript.

**Funding:** This research was funded by the BPI PIA4 DreamScanner project.

**Institutional Review Board Statement:** Not applicable.

**Informed Consent Statement:** Not applicable.

**Data Availability Statement:** The data presented in this study are available on request from the corresponding author. The data are not publicly available due to the confidentiality policy.

**Conflicts of Interest:** The authors declare no conflict of interest.

#### References

1. Kinahan, P.E.; Defrise, M.; Clackdoyle, R. Analytic image reconstruction methods. In *Emission Tomography: The Fundamentals of PET and SPECT*; Elsevier Academic Press: Cambridge, MA, USA, 2004; Chapter 20, pp. 421–442.
2. Lalush, D.S.; Wernick, M.N. Iterative image reconstruction. In *Emission Tomography: The Fundamentals of PET and SPECT*; Elsevier Academic Press: Cambridge, MA, USA, 2004; Chapter 21, pp. 443–472.
3. Maxim, V. Filtered backprojection reconstruction and redundancy in Compton camera imaging. *IEEE Trans. Image Process.* **2014**, *23*, 332–341. [[CrossRef](#)] [[PubMed](#)]
4. Parajuli, R.K.; Sakai, M.; Parajuli, R.; Tashiro, M. Development and Applications of Compton Camera—A Review. *Sensors* **2022**, *22*, 7374. [[CrossRef](#)] [[PubMed](#)]
5. Shepp, L.; Vardi, Y. Maximum Likelihood Reconstruction for Emission Tomography. *IEEE Trans. Med. Imaging* **1982**, *1*, 113–122. [[CrossRef](#)] [[PubMed](#)]
6. Parra, L.; Barrett, H.H. List-Mode Likelihood: EM Algorithm and Image Quality Estimation Demonstrated on 2-D PET. *IEEE Trans. Med. Imaging* **1998**, *17*, 228–235. [[CrossRef](#)] [[PubMed](#)]
7. Sato, Y.; Terasaka, Y.; Utsugi, W.; Kikuchi, H.; Kiyooka, H.; Torii, T. Radiation imaging using a compact Compton camera mounted on a crawler robot inside reactor buildings of Fukushima Daiichi Nuclear Power Station. *J. Nucl. Sci. Technol.* **2019**, *56*, 801–808. [[CrossRef](#)]
8. Geman, S.; Geman, D. Stochastic Relaxation, Gibbs distributions, and the Bayesian Restoration of Images. *IEEE Trans. Pattern Anal. Mach. Intell.* **1984**, *PAMI-6*, 721–741. [[CrossRef](#)] [[PubMed](#)]
9. Li, S.Z. *Markov Random Field Modeling in Image Analysis*, 3rd ed.; Advances in Pattern Recognition; Springer Science & Business Media: Berlin, Germany, 2009.
10. Green, P.J. Bayesian reconstructions from emission tomography data using a modified EM algorithm. *IEEE Trans. Med. Imaging* **1990**, *9*, 84–93. [[CrossRef](#)] [[PubMed](#)]

11. Lange, K. Convergence of EM image reconstruction algorithms with Gibbs smoothing. *IEEE Trans. Med. Imaging* **1990**, *9*, 439–446. [[CrossRef](#)] [[PubMed](#)]
12. De Pierro, A.R. A modified expectation maximization algorithm for penalized likelihood estimation in emission tomography. *IEEE Trans. Med. Imaging* **1995**, *14*, 132–137. [[CrossRef](#)] [[PubMed](#)]
13. Chang, J.H.; Anderson, J.M.; Votaw, J.R. Regularized image reconstruction algorithms for positron emission tomography. *IEEE Trans. Med. Imaging* **2004**, *23*, 1165–1175. [[CrossRef](#)] [[PubMed](#)]
14. Bouman, C.A.; Sauer, K. A Unified Approach to Statistical Tomography Using Coordinate Descent Optimization. *IEEE Trans. Med. Imaging* **1996**, *5*, 480–492. [[CrossRef](#)]
15. Le, N.; Snoussi, H.; Hmissi, M.Z.; Iltis, A.; Lebonvallet, G.; Zeufack, G. An extended list-mode MLEM algorithm for 3D Compton image reconstruction from multi-view data. In Proceedings of the 8th International Conference on Advancements in Nuclear Instrumentation Measurement Methods and Their Applications, Lucca, Italy, 12–16 June 2023.
16. Wilderman, S.J.; Clinthorne, N.H.; Fessler, J.A.; Rogers, W.L. List-mode maximum likelihood reconstruction of Compton scatter camera images in nuclear medicine. In Proceedings of the IEEE Nuclear Science Symposium Conference Record, Toronto, ON, Canada, 8–14 November 1998; Volume 3, pp. 1716–1720.
17. Barrett, H.H.; White, T.; Parra, L.C. List-mode likelihood. *J. Opt. Soc. Am. A* **1997**, *14*, 2914–2923. [[CrossRef](#)] [[PubMed](#)]
18. Qi, J.; Leahy, R.M. Iterative reconstruction techniques in emission computed tomography. *Phys. Med. Biol.* **2006**, *51*, R541. [[CrossRef](#)] [[PubMed](#)]
19. Zhang, H.; Wang, J.; Zeng, D.; Tao, X.; Ma, J. Regularization strategies in statistical image reconstruction of low-dose X-ray CT: A review. *Med. Phys.* **2018**, *45*, e886–e907. [[CrossRef](#)]
20. Bouman, C.A. *Foundations of Computational Imaging: A Model-Based Approach*; SIAM—Society for Industrial and Applied Mathematics: Philadelphia, PA, USA 2022.
21. Frandes, M.; Magnin, I.E.; Prost, R. Wavelet Thresholding-Based Denoising Method of List-Mode MLEM Algorithm for Compton Imaging. *IEEE Trans. Nucl. Sci.* **2011**, *58*, 714–723. [[CrossRef](#)]
22. Villain, N.; Goussard, Y.; Idier, J.; Allain, M. Three-Dimensional Edge-Preserving Image Enhancement for Computed Tomography. *IEEE Trans. Med. Imaging* **2003**, *22*, 1275–1287. [[CrossRef](#)] [[PubMed](#)]
23. Maxim, V.; Lojacono, X.; Hilaire, E.; Krimmer, J.; Testa, E.; Dauvergne, D.; Magnin, I.; Prost, R. Probabilistic models and numerical calculation of system matrix and sensitivity in list-mode MLEM 3D reconstruction of Compton camera images. *Phys. Med. Biol.* **2016**, *61*, 243. [[CrossRef](#)] [[PubMed](#)]

**Disclaimer/Publisher’s Note:** The statements, opinions and data contained in all publications are solely those of the individual author(s) and contributor(s) and not of MDPI and/or the editor(s). MDPI and/or the editor(s) disclaim responsibility for any injury to people or property resulting from any ideas, methods, instructions or products referred to in the content.